Human Molecular Genetics, 2007, Vol. 16, No. 14 ***1661–1675***
doi:10.1093/hmg/ddm114
Advance Access published on May 17, 2007

Filamin B mutations cause chondrocyte defects in skeletal development

Jie Lu[1], Gewei Lian[1], Robert Lenkinski[2], Alec De Grand[3], R. Roy Vaid[4], Thomas Bryce[4], Marina Stasenko[5], Adele Boskey[5], Christopher Walsh[6] and Volney Sheen[1,*]

[1]Department of Neurology, [2]Department of Radiology and [3]Department of Hematology and Oncology, Beth Israel Deaconess Medical Center, Harvard Medical School, Boston, MA 02115, USA, [4]Department of Radiology, University of California at San Francisco, CA 94305, USA, [5]Hospital for Special Surgery, Weill Medical College of Cornell University, New York, NY 10021, USA and [6]Howard Hughes Medical Institute, Program in Biological and Biomedical Sciences, Harvard Medical School, Boston, MA 02115, USA

Received January 9, 2007; Revised and Accepted April 26, 2007

Filamin B (FLNB) is a cytoplasmic protein that regulates the cytoskeletal network by cross-linking actin, linking cell membrane to the cytoskeleton and regulating intracellular signaling pathways responsible for skeletal development (Stossel, T.P., Condeelis, J., Cooley, L., Hartwig, J.H., Noegel, A., Schleicher, M. and Shapiro, S.S. (2001) Filamins as integrators of cell mechanics and signalling. *Nat. Rev. Mol. Cell Biol.*, 2, 138–145). Mutations in *FLNB* cause human skeletal disorders [boomerang dysplasia, spondylocarpotarsal (SCT), Larsen, and atelosteogenesis I/III syndromes], which are characterized by disrupted vertebral segmentation, joint formation and endochondral ossification [Krakow, D., Robertson, S.P., King, L.M., Morgan, T., Sebald, E.T., Bertolotto, C., Wachsmann-Hogiu, S., Acuna, D., Shapiro, S.S., Takafuta, T. *et al.* (2004) Mutations in the gene encoding filamin B disrupt vertebral segmentation, joint formation and skeletogenesis. *Nat. Genet.*, 36, 405–410; Bicknell, L.S., Morgan, T., Bonafe, L., Wessels, M.W., Bialer, M.G., Willems, P.J., Cohn, D.H., Krakow, D. and Robertson, S.P. (2005) Mutations in FLNB cause boomerang dysplasia. *J. Med. Genet.*, 42, e43]. Here we show that Flnb deficient mice have shortened distal limbs with small body size, and develop fusion of the ribs and vertebrae, abnormal spinal curvatures, and dysmorphic facial/calvarial bones, similar to the human phenotype. Characterization of the mutant mice demonstrated increased apoptosis along the bone periphery of the distal appendages, consistent with reduced bone width. No changes in the initial proliferative rate of chondrocytes were observed, but the progressive differentiation of chondrocyte precursors was impaired, consistent with reduced bone length. The extracellular matrix appeared disrupted and phosphorylated β1-integrin (a collagen receptor and Flnb binding partner) expression was diminished in the mutant growth plate. Like integrin-deficient chondrocytes, adhesion to the ECM was decreased in *Flnb* (−/−) chondrocytes, and inhibition of β1-integrin in these cells led to further impairments in cell spreading. These data suggest that disruption of the ECM-β1-integrin-Flnb pathway contributes to defects in vertebral and distal limb development, similar to those seen in the human autosomal recessive SCT due to *Flnb* mutations.

INTRODUCTION

Filamin proteins regulate the cytoskeletal network by cross-linking actin, linking the cell membrane to the cytoskeleton, and by regulating intracellular signaling and protein trafficking pathways responsible for development (1). Filamin A, B and C comprise a family of three actin-binding proteins, each sharing the common features of an N-terminal actin binding domain, followed by Immunoglobulin (IG) like repeat domains that contain the receptor binding region at the C-terminus (2). The proteins are highly homologous, can interact to form both homodimers and heterodimers and likely share similar

*To whom correspondence should be addressed at: HIM 858, Beth Israel Deaconess Medical Center, 77 Avenue Louis Pasteur, Boston, MA 02115, USA. Tel: +1 6176672699; Fax: +1 6176670800; Email: vsheen@bidmc.harvard.edu

functions across various organ systems. FLNA is predominantly found in the brain and blood vessels, FLNB in bone and FLNC in muscle. Insight into the function served by these proteins, however, has been limited to observations based on the human diseases, their expression patterns and isolated cellular and molecular culture studies—in large part due to the fact that null *Flna* and *Flnc* mice are embryonic lethal (3,4).

Filamin B (FLNB) has been shown to interact with numerous other proteins. These interactors demonstrate great functional diversity including (i) regulation of cortical actin networks through FLNB binding to actin, (ii) interaction with transmembrane receptors and signaling molecules such as filamin binding LIM protein-1 and β1-integrin (5–7) and (iii) serving as signaling scaffolds with intracellular proteins including presenilin (PS1 and PS2) (8). Moreover, FLNA is known to be expressed in developing chondrocytes, forms a heterodimer with FLNB (9) and has been shown to bind over 30 cellular interactors (reviewed in 2). Like FLNA, FLNB homodimers probably regulate the actin cytoskeleton through interactions derived from its multiple receptor binding regions, thereby regulating cell stability, protrusion and migration. In this respect, the actin binding protein likely orchestrates many ongoing fundamental cell–cell and cell–matrix interactions during bone development, and which interactions are relevant in organ development remain unclear (reviewed in 10).

To examine the cellular and molecular role of Flnb in skeletal development, we generated a *Flnb* knockout model in mice. Characterization of the viable mouse phenotype revealed impairments in bone growth, predominantly due to increased cell death along the perichondrium and disruption of chondrocyte progression through and differentiation in the hypertrophic zone-features similar to those seen in the β1-integrin and collagen deficient mice. Moreover, the mutant mice show abnormalities in the extracellular matrix and β1-integrin function. Reduced proteoglycan expression and increased collagen fibril density in the null *Flnb* mice are consistent with a disruption in the extracellular matrix. Flnb binds β1-integrin and phosphorylation of β1-integrin in the chondrocytes of these mice was diminished. Finally, the impairments in cell adhesion to extracellular matrix proteins seen in cultured Flnb-deficient chondrocytes were further enhanced with inhibition of β1-integrin. Our results show that filamin protein interactions with the extracellular matrix and integrin receptors are necessary components for chondrocyte survival and differentiation.

RESULTS

Loss of Flnb leads to impaired murine growth

Mice that are deficient in Flnb were generated by targeted deletion of exons 3–5 of the *Flnb* gene using a Neo gene cassette. The homologous recombination caused a predicted frameshift and early truncation mutation (Fig. 1A). Integration of the *Flnb* construct into 129 ES cell lines was confirmed by Southern blot analysis (Fig. 1B). Genotyping of mice were performed by PCR tailing of genomic DNA (Fig. 1B, lower panel) and the graded loss of Flnb protein expression in heterozygous and homozygous mice was confirmed by western blot analysis (Fig. 1D). Flnb was expressed across the entire growth plate and was absent in the null *Flnb* mice at embryonic day 16.5 (E16.5) (Fig. 1C). Genotyping data from the mice breeding studies suggested that a significant portion of the null *Flnb* (−/−) mice were embryonic or early postnatal lethal. Of the pups born and genotyped within the first week of life, 7.7% were homozygous, 65% were heterozygous and 27.3% were wild-type ($n = 297$, $P <= 0.001$ by χ^2 test). No differences were observed in the numbers of homozygous male and females born. The homozygous male *Flnb* (−/−) mice largely appeared healthy and fertile but displayed a stunted growth similar to the dwarfism associated with the human disorders harboring both dominant and recessive mutations in this gene (Fig. 2A and B). A similar trend was seen in the female mice, but was not statistically significant. *Flnb* (−/−) mice also exhibited a reduced growth rate that was captured by comparison of the body weights of littermate wild-type (WT) and null *Flnb* mice (Fig. 2B and C). Given a slower growth rate throughout development, the *Flnb* (−/−) male mice never reached the comparable size of counterpart adult WT mice (by 8 weeks of age).

Delay in endochondral bone development in null *Flnb* mice

FLNB mutations in humans can cause vertebral, carpal and tarpal fusions, joint dislocations, craniofacial abnormalities, poorly modeled appendicular bones and disharmonious skeletal maturation (11). We therefore examined the skeletal profile of male *Flnb* (−/−) mice by histological staining and standardized micro-CT scanning (12). Skeletal preparations stained with Alizarin red and Alcian blue showed that embryonic day 18.5 (E18.5) *Flnb* (−/−) mice had hypoplastic cartilaginous skeletons and delayed endochondral and intramembranous ossification, consistent with the overall reduction in body size compared with WT (Fig. 3A). Micro-CT scans of *Flnb* (−/−) mice at various developmental ages demonstrated a generalized mottled osteopenia and demineralization of the skeleton (Fig. 3B). Several of the trabecular and cortical bones (calvaria, patella and appendicular limbs) appeared to be poorly calcified as evidenced by the diminished radiolucency on CT scan. Mice had dysmorphic facial bones and calvaria, and the ribs appeared thin and gracile. In addition, multiple skeletal defects including abnormal fusion of the proximal ribs and fusion of cervical spinal vertebrae were seen in some *Flnb* (−/−) mice. Other null *Flnb* mice had exaggerated lower thoracic lordosis and exaggerated thoracolumbar kyphosis. Bone densitometry measurements of the vertebral segments indicated a significant reduction in bone density and ossification (Fig. 3C) in the mutant mice. The reduced bone ossification in the *Flnb* (−/−) mice was also apparent by von Kossa staining, where the ulna and radius appeared thinned and more fragile (Fig. 3D). These findings are consistent with a delay in skeletal development.

During skeletal formation, the growth plates (G) of the appendicular bones are composed of chondrocytes in different developmental stages. Each stage is reflected by a different zone, extending from the resting (R), to the proliferative (P) and lastly, to the hypertrophic (H) zones (13). Chondrocytes transitioning from the resting to the proliferative stage divide, rotate and are pushed longitudinally in columns into

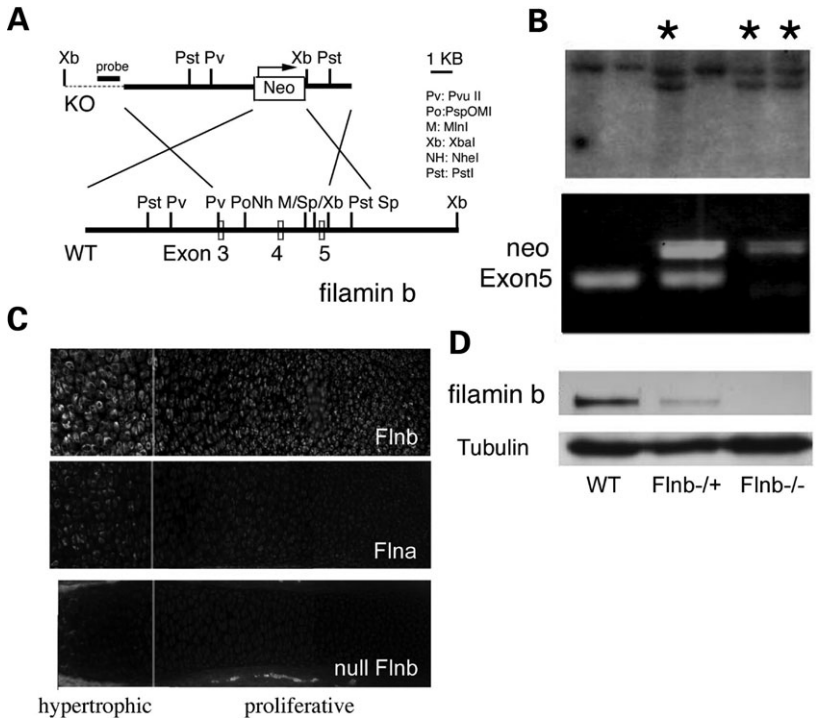

Figure 1. Generation of homozygous *Flnb* (−/−) mice. (**A**) Schematic of the genomic wild-type and targeted alleles, and the targeting vector. White boxes represent exons and restriction sites are indicated. In this strategy, the Neo gene cassette replaces exons 3–5, which will cause a frame shift mutation. (**B**) Southern-blot of genomic DNA from individual ES cell clones. The genomic DNA was digested using the *Xba*I restriction enzyme. The expected size of the wild-type allele is 11.5 kb and the knockout allele is 9 kb. The asterisks indicate identified recombinant clones. PCR analysis of genomic DNA isolated from mice toe clippings. A 3 kb band amplifying the (NEO) cassette and the 2.6 kb band amplifying (Exon5) allowed for identification of homozygous knockout and wild-type mice, respectively. (**C**) Fluorescent photomicrographs demonstrating spatial localization of Flnb (fluoroscein) to the entire growth plate of the radius, restricted expression of Flna (rhodamine) to the hypertrophic zone and absence of Flnb expression in the null *Flnb* mice. (**D**) Western blot of Flnb expression from P7 livers of WT (wild-type), heterozygous *Flnb* (+/−) and homozygous *Flnb* (−/−) mice shows appropriate, graded loss of Flnb protein expression in the heterozygous and null mice.

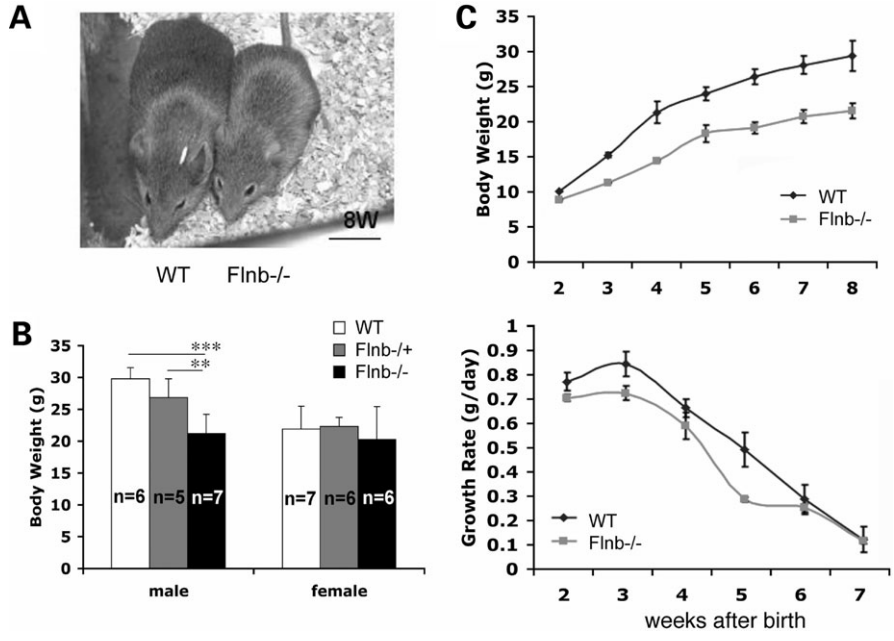

Figure 2. Retarded skeletal growth in homozygous *Flnb* (−/−) male mice. (**A**) Gross appearances of wild-type and *Flnb* (−/−) mice at 8 weeks (8W) of age. (**B**) The reduction in body weight of heterozygous *Flnb* (+/−) and homozygous *Flnb* (−/−) mice when compared with WT mice at 8 weeks of age was graphically quantified (±SD; $^{**}P < 0.01$; $^{***}P < 0.001$ by *t*-test). (**C**) Dynamic change of body weight (upper) and growth rate (lower) in male mice over an 8 weeks course of development (±SEM). In comparison with littermate controls, *Flnb* (−/−) mice showed significant decreases in body weight and growth rate. Scale bar in (A) = 20 mm.

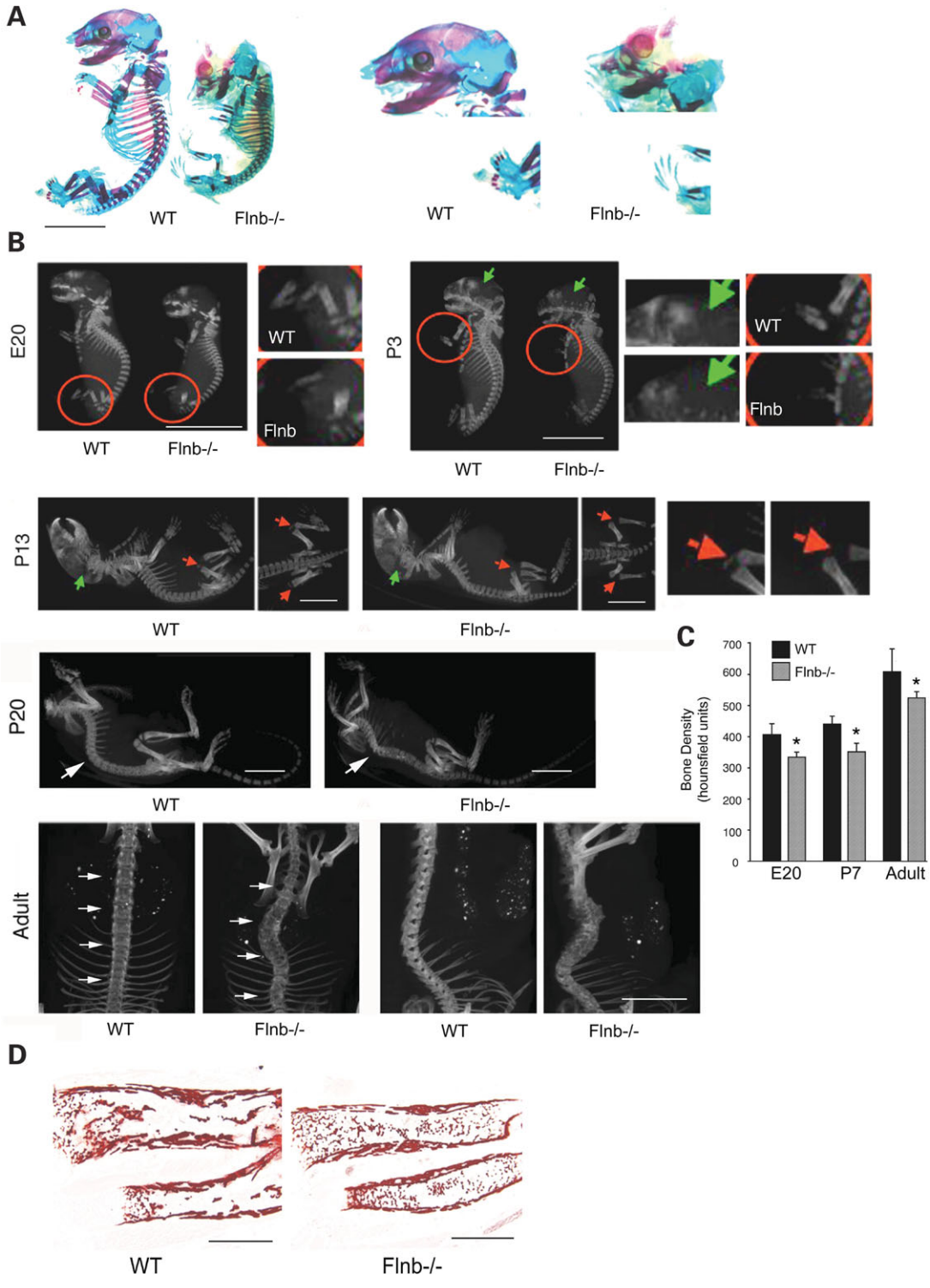

Figure 3. Delayed bone calcification and ossification in homozygous *Flnb* (−/−) mice. (**A**) Whole skeleton preparation of embryonic day (E) 18.5 WT and *Flnb* (−/−) embryos, stained with Alizarin red (bone) and Alcian blue (cartilage), show a decrease in bone mineralization. Enlarged corresponding images are to the right. (**B**) Micro-CT scans of WT and *Flnb* (−/−) mouse skeletons at different ages [E20, postnatal day (P) 3, P13, P20 and Adult]. Compared with controls, the parietal and occipital bones (green arrow), limbs (red circle) and patellar bones (red arrow) of Flnb deficient mice were also poorly calcified. In addition, the thoracic cages were both smaller and demonstrated increased radiolucency suggestive of osteopenia, consistent with impaired calcification and ossification. Enlarged images are to the right. Lastly, older mutant mice develop fusion of the vertebrae (P20, white arrow) and abnormal spinal curvature with kyphosis or scoliosis (Adult, white arrows). (**C**) Bone densitometry measurements from the vertebrae of E20, P7 and adult *Flnb* (−/−) mice by CT scan showed decreased bone density compared with wild-type mice. The error bars (standard deviation) refer to the degree of variation seen in Hounsfield unit measurements of all voxels within that volume ($^*P < 0.05$ by Student *t*-test). (**D**) The ulna (upper) and radius (lower) of Flnb deficient mice were less calcified and more fragile appearing by von Kossa staining when compared with wild-type mice. Scale bars in (A) = 5 mm, (B) = 10 mm, (D) = 500 μm.

the hypertrophic zone. These cells subsequently differentiate into hypertrophic chondrocytes and later undergo apoptosis and are replaced by osteoblasts to form bone. Mutations affecting chondrocytes (14–21), osteoblasts (22–24) or the bone matrix (25–27) can all cause dwarfism with shortened bones and skeletal abnormalities, as seen in these mutant mice. We therefore more closely characterized the appendicular bones of the forelimbs in male mice. The growth plates in E16.5 and adult *Flnb* (−/−) mice were significantly shortened compared with those in WT mice, although no gross changes were appreciated in the structural organization of chondrocytes (Fig. 4A). Moreover, the greatest reduction in length was observed in the more distal radius, ulna and digital bones, as opposed to the more proximal humerus (Fig. 4B), consistent with the human *FLNB* phenotype (11). Within the growth plate, mutant *Flnb* (−/−) chondrocytes in the hypertrophic (H) zone, and to a lesser extent in the P zone, were more severely affected, as these zones were significantly shortened in length (Fig. 4C). Additionally, *in situ* hybridization of the various collagen mRNAs in the forelimb appendages showed that the bone matrix and proliferative zone in the *Flnb* (−/−) mice were slightly decreased in length and width by collagen I and collagen II staining, respectively. Collagen X staining confirmed a clear reduction in the length and width of the hypertrophic zone (Fig. 4D and E). Finally, the boundaries of the Indian hedgehog (Ihh) and parathyroid hormone related protein receptor (Pthrpr) mRNA staining were slightly increased and more blurred in the mutant mice, suggestive of a possible delay in prehypertrophic to hypertrophic chondrocyte differentiation (Fig. 4F). Overall, characterization of the *Flnb* (−/−) skeletal abnormalities suggests an early defect effecting hypertrophic chondrocyte differentiation within the more distal rather than proximal appendages.

Chondrocytes lacking Flnb expression undergo increased cell death and exhibit delayed differentiation

To explore the cellular mechanisms underlying the abnormal chondrocyte development, we first evaluated whether there were any changes in ongoing cell death and proliferation within the growth plate. An increase in apoptosis was seen in the H zone of E16.5 radius, as shown by TUNEL (Fig. 5A). Increased rates of cell death occurred along the periphery of the radius bones within and were seen between E14.5 and E17.5 in the mutant mice. The dying cells were restricted primarily to the perichondral regions, adjacent to the hypertrophic zone. This increase in cell death also paralleled the impaired growth of the bone width in the hypertrophic zone (Fig. 5B). Furthermore, while proliferation in the P zone of E16.5 radius was largely unchanged (1 h post BrdU injection), the distribution of progenitors incorporating BrdU was shifted toward the resting zone in the mutant mice (Fig. 5C and D). This shift away from the H zone coincided with an increase in cell density in the areas more distal to the H zone, consistent with a potential delay in the progression of chondrocyte differentiation and progression through the H zone. To further address this change, we examined the distance traveled by BrdU labeled chondrocytes through the P zone. By 12 h, fewer BrdU positive cells in the null *Flnb* mice had progressed out toward the H zone (Fig. 5E). This delay coincided with a decrease in the length of the H zone of the E16.5 radius (Fig. 5F). Overall, the increased rates of chondrocyte cell death along the periphery of the forming bone would explain the decreased bone width but not the shortening of bone height. Rather, a delay in chondrocyte differentiation would be more consistent with the impaired ossification seen on Alzarin Red/Alcian blue staining, by micro-CT imaging and by von Kossa staining for bone.

Impairments in the extracellular matrix and β1-integrin pathway in Flnb-deficient mice

During development, chondrocytes are pushed along the differentiation columns by the increased matrix production and cell proliferation (interstitial growth). In the absence early on of any change in rates of proliferation, disruption of chondrocyte adhesion and proteoglycan synthesis could contribute to a shorter hypertrophic zone. We therefore examined hematoxylin and eosin, von Kossa and safranin-O stainings of the radial bone at various aged mutant and wild-type mice. While no clear changes were seen in chondrocyte rotation and column formation, the histology reflected a delay in the chondrocyte transitions from the proliferative to hypertrophic and ossification zones (Fig. 6A). For example, the radius of the E14.5 mutant mice has not yet developed an early, definable hypertrophic zone, when compared with the age-matched wild-type mouse (white bar). Furthermore, the ossification zone (black arrowhead), where dying chondrocytes are gradually replaced by osteoblasts/osteoclasts, is more developed in the wild-type mouse at E15.5 on hematoxylin and eosin staining. The von Kossa staining supports this observation as the radius in the Flnb-deficient mutant mouse is both shorter in length and thinner in width than the wild-type mouse at this age. Moreover, a reduction in safranin-O staining for proteoglycans was seen in the mutant mice suggesting a possible disruption in the extracellular matrix. Finally, electron micrographs of the developing bone also show that there was a disruption of the matrix, with prominent closely packed fibrils from E16.5 mutant mice (Fig. 6B). Collectively, these observations suggest that the delay in chondrocyte proliferation and/or differentiation may reflect some impairment involving the ECM.

Mice with impairments in the ECM or integrin exhibit similar features related to those seen in the *Flnb* (−/−) mice (14,25,26,28). Almost uniformly, there is a reduction in the size of the H zone in these mice, presumably reflecting a disruption in chondrocyte differentiation. The size of the prehypertrophic zone is variable and often blurred, as in the null *Flnb* mice. In addition, β1-integrin is highly expressed in chondrocytes (29), binds collagen and proteoglycans and interacts with the carboxyl terminal of FLNB (7,30,31). We therefore examined whether some disruption in the ECM-β1-integrin pathway could contribute to the null *Flnb* mouse phenotype. Consistent with previous studies, we found that GST-β1-integrin was able to pull-down both myc-FLNA and FLNB, expressed in 293 cells and that β1-integrin co-localized with Flnb along the chondrocyte cell periphery (Fig. 7A). In addition, fewer phospho-β1-integrin (Ser785) positive chondrocytes were observed in the radius of E16.5

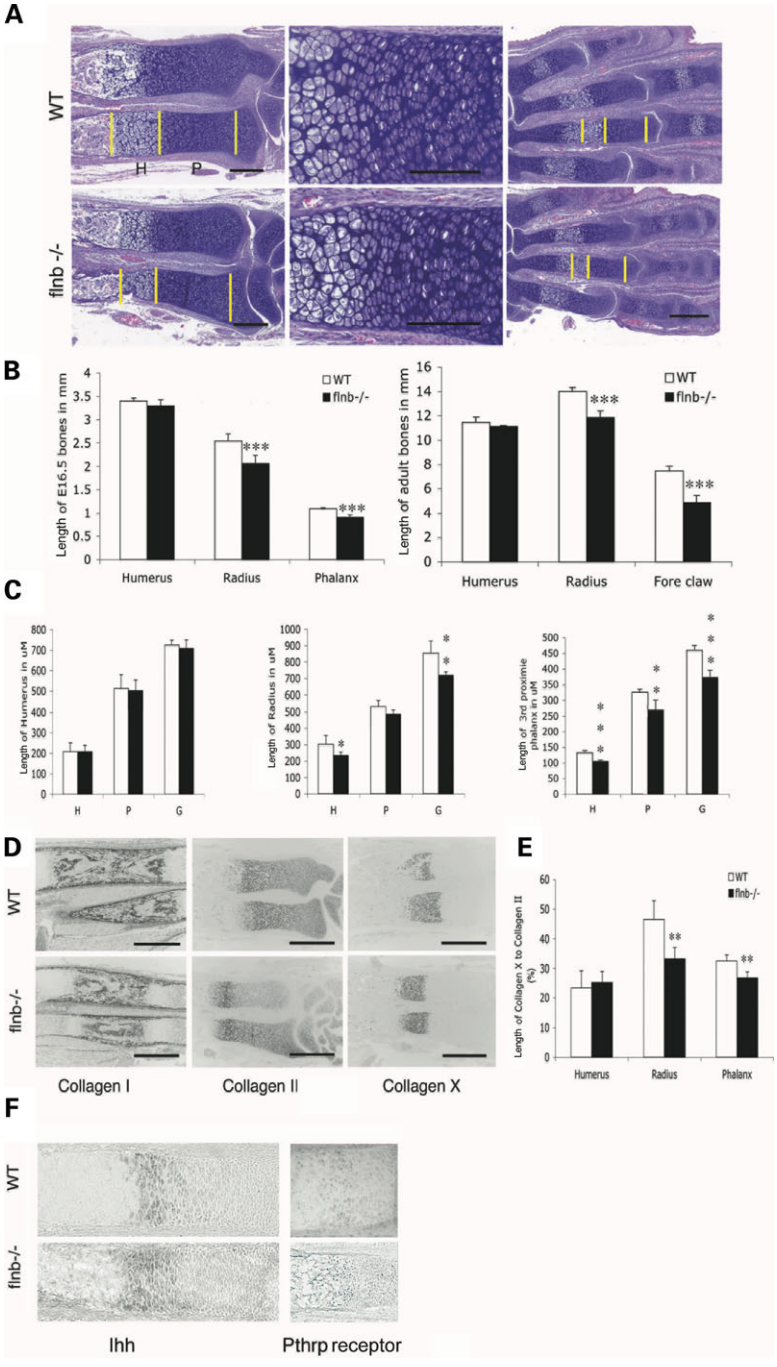

Figure 4. Shortening of distal skeletal appendages due to abnormal chondrocyte and bone matrix development in *Flnb* (−/−) mice. (**A**) Hematoxylin and eosin staining of E16.5 distal bone appendages in WT and *Flnb* (−/−) mice. Growth plates of mutant mice were smaller than counterpart wild-type mice, as shown in the ulna, radius (left lane) and phalanx (right lane). Chondrocyte size and shape were not significantly different between experimental and control mice (middle lane, higher magnification of radius). No abnormalities in chondrocyte rotation and column integrity were seen. (**B**) Lengths of the humerus, radius and phalanx from E16.5 and 2-month-old adult mice were summarized graphically. The radius and phalanx were significantly shorter in mutant mice. (**C**) Detailed measurements of the different zones in the growth plates (G) as shown in (A) and (B). The greatest degree of shortening affected chondrocytes within the hypertrophic (H) zone, more so than cells in the proliferative (P) zone. (**D**) Collagen expression patterns in the ulna and radius of E16.5 WT and *Flnb* (−/−) mice by *in situ* hybridization. A reduction in bone matrix length and width, as shown by loss in collagen I expression, was seen in the *Flnb* (−/−) mice compared with control. The reduction in length of the H zone was confirmed by collagen X staining. A slight decrease in the length of the proliferative zone was appreciated by collagen II staining. (**E**) The length of the H zone was decreased in both the radius and phalanx of the Flnb deficient mice, when compared with WT mice, by measuring the collagen X-stained bone lengths (normalized to the collagen II stained bone lengths at various mice ages). (**F**) Increased length and blurring of the boundaries demarcating the prehypertrophic were seen with Indian hedgehog staining (and to a lesser extent with Pthrp receptor staining) *in situ* hybridization. $^{*}P < 0.05$, $^{**}P < 0.01$, $^{***}P < 0.001$. Scale bars in (A) = 250 μm, in (D) = 500 μm.

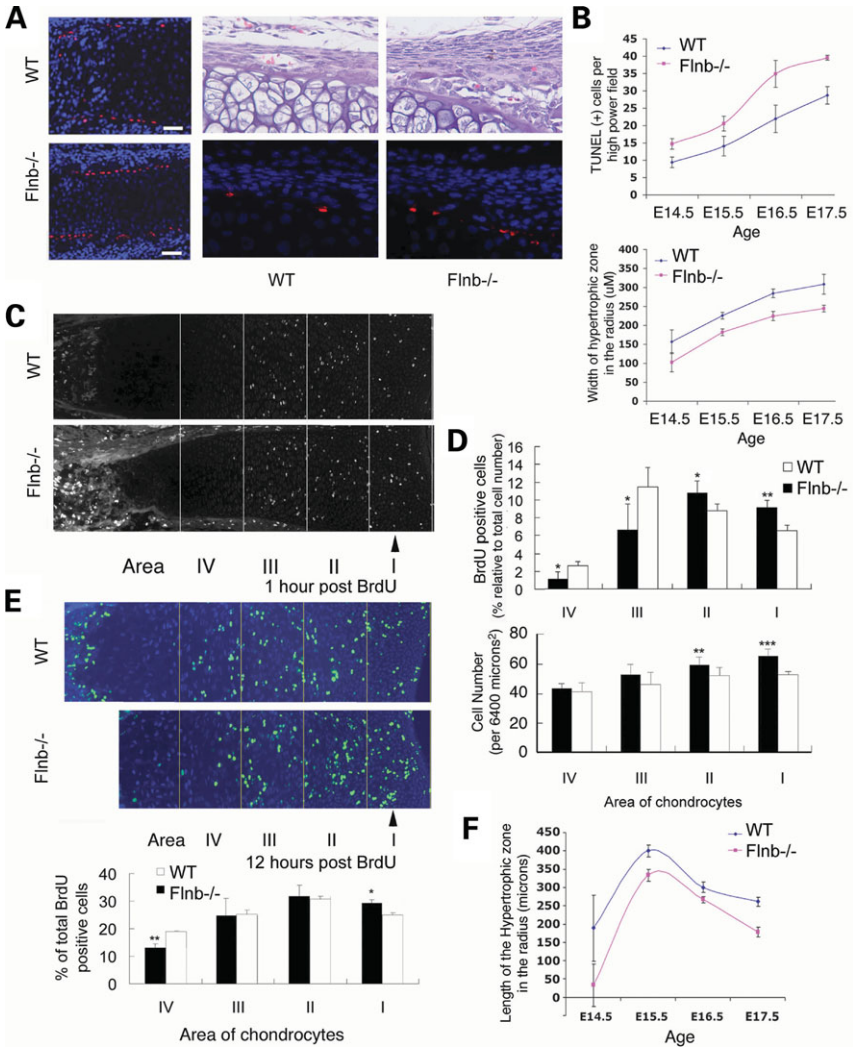

Figure 5. Enhanced apoptotic cell death and altered chondrocyte proliferation in homozygous *Flnb* (−/−) mice. (**A**) Increased programmed cell death by TUNEL staining (rhodamine fluorescence) was seen along the periphery of the H zone of the radius in E16.5 mutant mice. Sections were counterstained with the nuclear Hoechst stain (blue fluorescence). Higher magnification images to the right show that apoptotic cells reside within the perichondrium, adjacent to the hypertrophic zone. (**B**) The increase in cell death was noted along the bone collar and was consistently seen through all skeletal developmental ages. This increase paralleled the decrease in bone width seen in the *Flnb* mutant mice. (**C** and **D**) Overall rates of proliferation were unchanged between WT and mutant mice 1 h after BrdU incorporation. However, the distribution of proliferating chondrocyte progenitors (rhodamine fluorescence) in null *Flnb* mice were localized more distal to the H zone (Areas I and II), as compared with WT chondrocyte progenitors (Areas II and III). These same regions also demonstrated an increased density of chondrocyte progenitors. This asymmetric shift would be consistent with a delay in chondrocyte progression and differentiation in the H zone. (**E**) This delay in chondrocyte progression was also seen 12 h after the BrdU pulse. Fewer chondrocytes (fluoroscein fluorescence) in the mutant mice had progressed toward the hypertrophic zone (adjacent to area IV) when compared with wild-type control. BrdU labeled osteoblasts were appreciated further distal to the proliferative zone (far left). (**F**) The greatest differences in the length of the hypertrophic zones between wild-type and mutant mice occurred earlier at E14.5 and E15.5, suggestive of a delay in chondrocyte maturation and hypertrophy. $^{*}P < 0.05$, $^{**}P < 0.01$, $^{***}P < 0.001$. Scale bar in (A) = 125 μM.

Flnb (−/−) mice (Fig. 7B). Western blot analyses of dissociated chondrocyte cultures also showed a reduction in phospho-integrin protein expression within the mutant mice (Fig. 7C). Loss of β1-integrin phosphorylation at Ser785 has been shown to inhibit cell adhesion (32). Consistent with this finding, Flnb deficient chondrocytes also exhibited decreased adhesion to several extracellular substrates including collagen and fibronectin (Fig. 7D). The null *Flnb* chondrocytes also showed diminished binding to other ECM components (i.e. type IV collagen, vitronectin and laminin) that do not bind β1-integrin. While these results suggested that Flnb could be involved in multiple pathways that regulate receptor-ECM interactions, inhibition of β1-integrin could still exacerbate the loss of function phenotype (i.e. altered cell adhesion). Thus, to further confirm the disruption of the β1-integrin–Flnb interaction, we transfected cultured chondrocytes with a dominant negative β1-integrin construct (integrin-Δ) and assessed changes in cell adhesion, by gauging changes in cell surface area. At baseline, *Flnb* (−/−) chondrocytes demonstrated reduced cell spreading compared with WT chondrocytes. Decreased adhesion within the Flnb deficient cells was further decreased by dominant negative

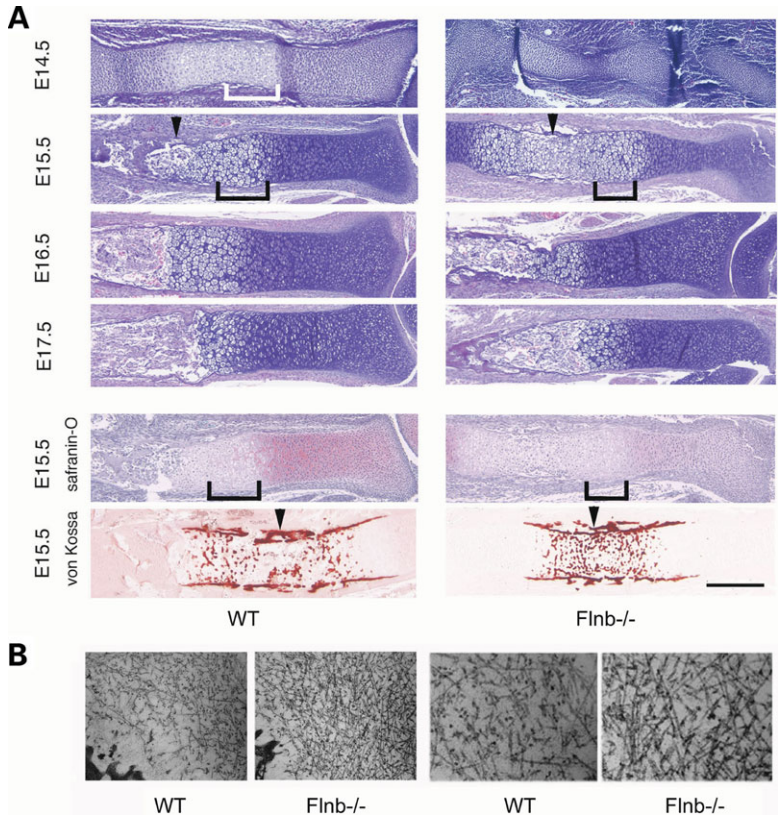

Figure 6. Impairments in the extracellular matrix coincide with delayed chondrocyte differentiation in *Flnb* mutant mice. (**A**) Hematoxylin and eosin stained sections from the radius of various aged wild-type and mutant *Flnb* mice. At E14.5, the proliferative zone was smaller in the mutant mouse and the hypertrophic zone had yet to form (white bar in the wild-type mouse) when compared with the control. A similar delay was seen at E15.5, where the hypertrophic regions showed diminished length in the knockout mice (black bars) and von Kossa staining for bone also showed decreased ossification (arrowheads). The mineralized portion of the radius in the mutant *Flnb* mouse is both shorter in length and thinner in width compared with the age-matched wild-type mouse. By E16.5, both the length and the width of the hypertrophic zone are significantly smaller in the mutant *Flnb* mice. This impaired growth is further confirmed on safranin-O staining for proteoglycans, demonstrating a smaller hypertrophic zone. The safranin-O staining in the *Flnb* (−/−) mice was also significantly weaker suggesting a disruption in the proteoglycan ECM. (**B**) Electron micrographs of the matrix compartments of wild-type and mutant growth plates at the E16.5 stage. The collagen fibril density was increased in *Flnb* (−/−) mice compared with that in wild-type. These findings also suggest that there is a disruption of the ECM. Scale bar = 500 μm.

β1-integrin transfection when compared with either Flnb deficient chondrocytes or WT chondrocytes transfected with the dominant negative β1-integrin alone (Fig. 7E). These findings suggest that the effects of Flnb and integrin inactivation are additive, and indicate that the two may act together.

DISCUSSION

In the present study, we show that loss of Flnb results in impaired mouse skeletal growth, leading to a smaller body size, shortened appendicular bones as well as thinning of the bones and abnormal bone fusions. These abnormalities result from a delay in chondrocyte development due to a progressive delay in differentiation within the hypertrophic zone, and an increase in cell death along the perichondrium. The null mice also exhibit increased fibril density and decreased proteoglycan expression suggestive of some disruption in the ECM. Physical interactions and functional studies indicate that Flnb binds to and co-localizes with β1-integrin, can impair β1-integrin activation and decrease chondrocyte adhesion along the ECM. Taken in sum, the delayed ossification in Flnb deficient mice may, in part, reflect a similar pathogenesis seen with disruption of the ECM-integrin pathway through loss of cell adhesion, thereby effecting chondrocyte differentiation and anoikis.

The complete loss of Flnb function in mice provides a comparative model for the genotype–phenotype correlations seen in humans who harbor recessive mutations in this same gene. The human autosomal recessive spondylocarpaltarsal synostosis syndrome (SCT, OMIM 272460) has been shown to result from the complete absence or truncation of FLNB (11,33,34). SCT has been associated with the unique constellation of findings including shortened stature, vertebral fusions and carpal coalition. More variably loss of gene function can lead to scoliosis/lordosis, joint laxity and rib anomalies (35–37). Loss of Flnb in mice similarly results in stunted growth, vertebral fusion and shortening of the distal bones, although no clear carpal coalition was observed. Analogous to the human counterpart, these mice also variably develop abnormal spinal curvature, joint laxity and rib anomalies. Overall, the high degree of genotypic–phenotypic correlation seen between

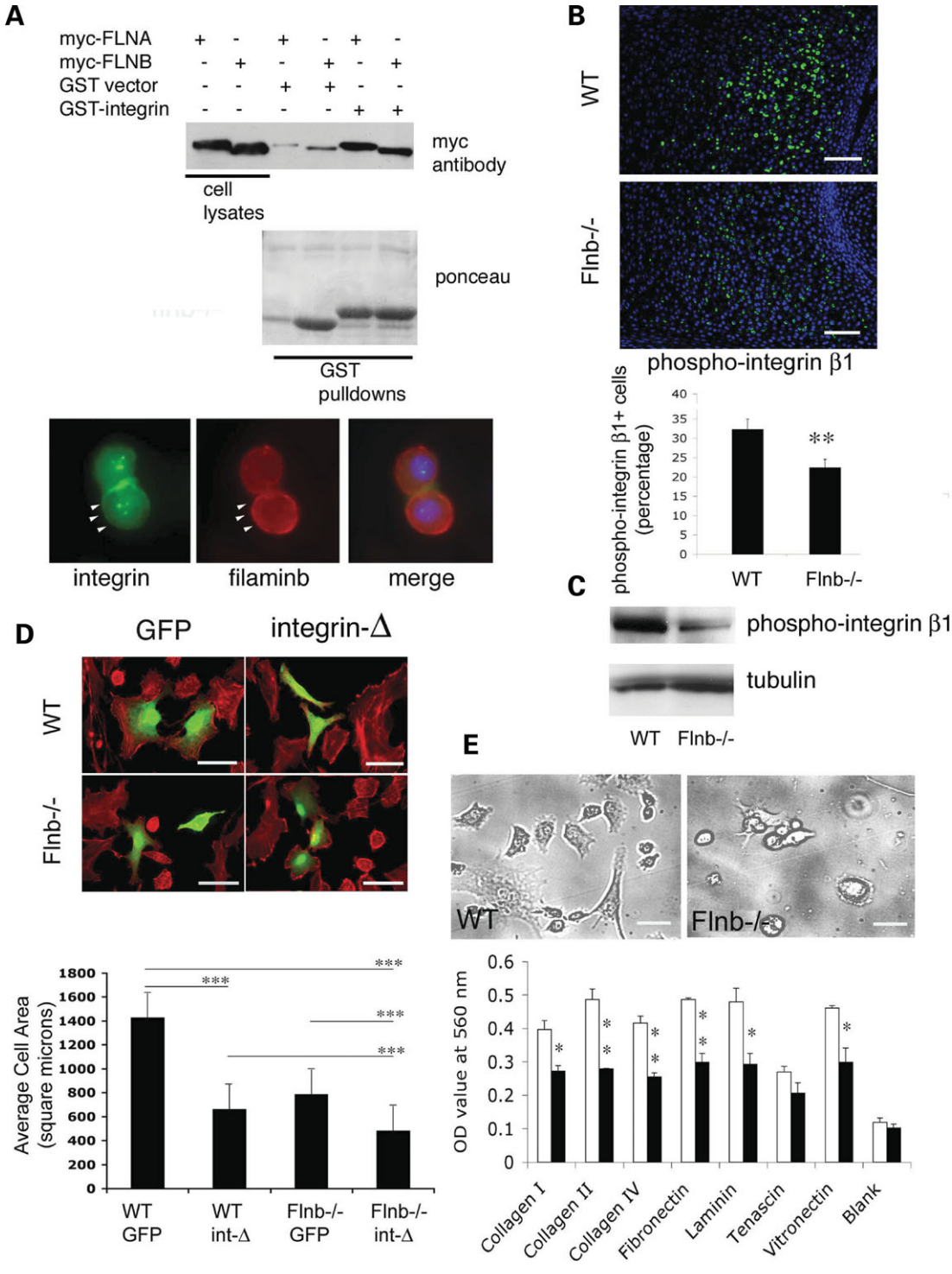

Figure 7. Flnb interactions with β1-integrin in chondrocytes. (**A**) Flnb bound β1-integrin by GST-pulldown and both proteins were co-localized to the peripheral cell membranes of chondrocytes (arrowheads). (**B**) Expression of the activated phospho-integrin β1(Ser 785) was decreased in the radius of *Flnb* (−/−) mice. (**C**) Phospho-integrin β1 expression was also reduced in chondrocytes cultured from *Flnb* (−/−) mice by western blot analyses and comparison with control. Phosphorylation of Ser785 is required for chondrocyte cell adhesion. (**D**) Null *Flnb* chondrocytes exhibited decreased cell adhesion and spreading compared with wild-type controls. Transfection of dominant negative integrin β1 (integrin-Δ) plasmid into *Flnb* (−/−) chondrocytes further hindered cell adhesion and spreading, as shown by measurements of cell surface area following phalloidin staining of actin. Average cell areas were quantified following transfection of GFP alone or integrin-Δ into WT or null *Flnb* chondrocytes. Results are graphically summarized. (**E**) Loss of Flnb function also led to diminished chondrocyte cell adhesion onto several extracellular matrix substrates. The phase-contrast photomicrographs above show that the mutant chondrocytes adopted more rounded morphologies after plating onto the adhesive molecules. Both WT and Flnb deficient chondrocytes were plated onto various adhesion ligands, stained and degree of cell adhesion was measured by absorbance at 550 nm. Results are graphically summarized. Asterisks $^{*}P < 0.05$, $^{**}P < 0.01$, $^{***}P < 0.001$. Scale bars in (B) = 250 μM, (D) = 50 μM, (E) = 12.5 μM.

mice and humans with this recessive disorder suggests that these anomalies can be attributable to complete loss of filamin b function.

Shared phenotypes between complete loss of *Flnb* function in the mutant mice and specific *FLNB* point mutations in the human autosomal dominant skeletal dysplasias provide a means with which to understand particular functional domains of this scaffolding protein. For example, human mutations in exons 2/3 (the calpain homology 2 domain) and exons 28/29 (repeats 14 and 15) of the *FLNB* gene essentially give rise to a spectrum of similar autosomal dominant skeletal dysplasias [Larsen syndrome (LS, 150250), type I atelosteogenesis (AOI; 108720), type III atelosteogenesis (AOIII; 108721) and boomerang dysplasia (BD, 112310)] (11,33,34). While segregated into distinct syndromes, these disorders share clear overlapping features. All of the dysplasias are characterized by short stature, either shortening/tapering or absence of the skeletal bones, and multinucleated giant cells. While Flnb deficient mice do develop short stature and shortening of the skeletal bones, these mice do not exhibit complete absence of skeletal bones or multinucleated giant cells, suggesting that disruption of the calpain homology 2 domain and IgG-like repeats 14 and 15 likely result in some gain of function. Moreover, the mutant mice largely do not share the distinguishing features for each of the particular syndromes. The null *Flnb* mice do not exhibit the short, bowed and rigid limbs and multinucleated giant cells seen in BD (33,38), the tapering of skeletal bones in AOIII, the complete absence of skeletal bones in AOI (39) and the recurrent joint dislocations in LS (although they do appear to have pelvic laxity seen during birthing) (40,41). As FLNB serves largely as a scaffold that regulates interactions between proteins and the actin cytoskeleton, specific point mutations in the gene may disrupt the regulation of particular pathways and result in both gain and loss of function.

Recent studies have reported the generation of another Flnb-deficient mouse produced by gene-trap insertion, and these mice exhibit clear differences in phenotype in comparison with mice generated in these experiments (42). Fewer than 3% of the Zhou *et al*. mice survive to term and they display severe skeletal and vascular malformations, not seen in the current studies. Several factors may account for these discrepancies in phenotype. The Zhou *et al*. mice were generated from a mutant embryonic stem cell line containing an in-frame, insertional mutation at intron 20. In this gene-trap approach, it is likely that a truncated protein is formed (containing exons 1–19), leading to a potential gain of function. In contrast, the Flnb-deficient mice used in the present studies were specifically designed to produce an early truncation mutation (prior to exon 3) and a loss of function. Differences in genetic background (BCB085 strain 129/Ola × C57BL/6 in the Zhou *et al*. mice and 129/SvEv × C57BL/6 in the current mice) may provide an alternative explanation as well. Interestingly, the current *Flnb* mutant mice share greater similarities to the human autosomal recessive SCT disorder, whereas the Zhou *et al*. mice appear to exhibit more severe phenotypes with early embryonic lethality, potentially more representative of the autosomal dominant *FLNB* human disorders. In addition, the Flnb mutant mice in the current experiments do not appear to exhibit any vascular defects but mutations in Flna have been shown to result in a vasculopathy and embryonic lethality. A potential Flnb gain of function could alter previously reported interactions between Flna and Flnb (18), disrupt Flna function and contribute to abnormalities in blood vessel formation.

Loss of filamin function in general contributes to abnormalities in skeletal development. Recent studies have shown that Flna-deficient mice have a sternum defect with a failure to fuse during embryonic development. Moreover, mutant males and some carrier females develop incomplete fusion of the palatal shelves leading to a cleft palate (3,4). While the Flnb-deficient mice do not develop these same abnormalities, these mice exhibit delays in endochondral development, primarily leading to a progressive dwarfism in males. Shortening of the distal appendages, thinning of these bones and abnormal fusion of the spinal vertebrae are the most prominent features seen with loss of *Flnb* gene function. Interestingly, Flna may play a greater role in intramembranous bone formation, given the defects seen in the palate, whereas Flnb appears to regulate endochondral ossification. This distinction is consistent with their partial non-overlapping patterns of expression. Flnb but not Flna is expressed within the early proliferating chondrocytes. Flna is more restricted to the hypertrophic zone chondrocytes and osteoblasts/osteoclasts.

Several observations support interactions between the integrin and filamin proteins. Consistent with our findings, Flna and Flnb have been shown to bind to β1-integrin (7,43). Disruption of Flna and β1-integrin interactions also appear to alter membrane protrusion and migration (43), suggesting that inhibition of Flnb function could result in a similar loss of function through β1-integrin. Although Flnb deficient mice show no clear abnormalities in myogenesis (data not shown), overexpression of Flnb and binding of Flnb to integrins are suggested to promote myocyte fusion, differentiation and formation of myotubes (7). Moreover, many of the same chondrocyte defects seen in the Flnb deficient mice mirror those seen following inhibition of β1-integrin. Loss of α5β1-integrin inhibits prehypertrophic chondrocyte differentiation (44). Blockade of β1-integrin leads to altered collagen deposition, smaller chondrocytes and increased apoptosis (45). Loss of integrin-linked kinases and β1-integrin also cause defects in adhesion, failure to spread and abnormal shape (28,46). The current studies also clearly show a decrease in β1-integrin phosphorylation at Ser785, which has been implicated in cell adhesion following phosphorylation. That said, the null β1-integrin chondrocytes show impairments in chondrocyte rotation, aberrant column formation and increased cell death within the proliferative zone; findings not observed in the Flnb mutant mice. The absence of these findings could reflect the fact that the Flnb mice do not appear to be severely affected as the β1-integrin deficient mice. This mitigated phenotype would be consistent with the observation that the filamin proteins likely serves as a scaffold to help anchor the integrin receptors near the cell surface, and loss of this function would not likely lead to complete loss of integrin function. Overall, Flnb may serve to transduce interactions between the ECM and integrins onto the actin cytoskeleton and thereby regulate chondrocyte differentiation.

While the *Flnb* mutant mouse show clear abnormalities in the ECM and chondrocyte adhesion, the disruption of

filamin–integrin interactions likely account for only part of this phenotype. In the current study, the null *Flnb* chondrocytes adhere poorly to many substrates, even those that do not depend on β1-integrin. One possible explanation, according to an inside-out signaling model for integrin activity, is that inactive, low affinity receptors are clustered through interactions with several cytoskeleton molecules such as actin, myosin and filamin. After ligand binding to integrin, these receptors could become activated with increased affinity for ECM ligands (47). This may place the cytoplasmic domain of β1-integrin as a key effector in establishing cell contacts, while its binding partners such as filamin regulate these activities. In this model, integrins could establish adhesion even though some of the ECM ligands may not function directly through the receptor. However, it is equally likely that filamin serves as a scaffold to other receptors involved in cell adhesion and disruption of this scaffolding leads to altered cell–matrix contacts. In this regard, the filamin proteins have already been implicated in modulating the endocytosis of different receptors (48). Similarly, the diminished safranin-O staining and closely packed fibrils seen in the mutant mice would indicate a problem in the proteoglycan ECM. While this abnormality may partially reflect problems in integrin to ECM signaling through Flnb, it remains to be seen whether filamin directly or indirectly affects proteoglycan glycosylation and/or secretion.

Mechanisms behind some phenotypic features observed in the null *Flnb* phenotype remain to be answered. It is unclear why female *Flnb* (−/−) mice are not as severely affected, although potentially their inherently smaller size may limit the distress placed on skeletal growth. Alternatively, functional redundancy from the X-linked *Flna* gene and its interactors may be different in females than in males (49). Factors leading to increased cell death are also not well understood. Flnb may help maintain cell–extracellular matrix contacts that facilitate chondrocyte survival through the integrin-dependent FAK/PI3K/Akt or MAPK pathways (11). Thus, the disruption of β1-integrin binding to *Flnb* (−/−) chondrocytes could partly account for the increased apoptosis in chondrocytes along the bone collar, although the increased cell death is not seen elsewhere. Furthermore, the skeletal defects appear less severe than that seen with the β1-integrin deficient mice and some of the phenotypic findings (fused vertebrae and ribs, abnormal spinal curvature, embryonic lethality) are variable, although this appears to be the case in humans with *FLNB* mutations as well. These differences may arise from compensatory interactions with other integrins (the integrin αdeficient mice have less severe skeletal abnormalities presumably from involvement of the β-integrins), and the heterodimeric interactions with Flna, which is also found in bone. Alternatively, Flnb likely binds to numerous other factors in its regulation of the actin cytoskeleton and these interactions may offset parallel pathways involved in skeletal development. Finally, the increased staining for Ihh and Pthrp receptor would generally suggest an increase in the prehypertrophic chondrocytes that are committed to becoming hypertrophic chondrocytes, thereby leading to an enlargement of the H zone. The mutant mice, however, clearly show a delay in endochondral calcification and a reduction in the length of the H zone. Mechanistically, this discrepancy could be explained by loss of Flnb function in altering or delaying chondrocyte terminal differentiation and cell fate at the prehypertophic/hypertrophic boundary as has been seen with blocking of α5β1-integrin (44). Alternatively, loss of Flnb could also disrupt the chondrocyte progenitors and the negative feedback mechanisms that regulate their proliferation and initiate the differentiation pathway.

The developmental defects seen in the various filamin deficient mice do provide a context with which to view filamin-dependent mechanisms. The null *Flna* mice exhibit aberrant vascular and skeletal patterning with disruption of the endothelial organization and adherens junction formation. These defects may in part be attributed to plexinD1 and ephrin-B1/B2 interactions with Flna which may act downstream of these receptors to regulate cell–cell contacts and adherens junction formation (Feng and Walsh, personal communications). This possibility is consistent with the observation that mutations in *ephrin-B1* result in a similar skeletal disorder, craniofrontonasal syndrome (49). The null *Flnb* mice also demonstrate abnormal skeletal development with disruption of cell adhesion and spreading, partially through interactions between Flnb and β1-integrin, again suggesting that Flnb may act downstream of this receptor to regulate cell–cell contacts and chondrocyte morphology. Interestingly, the RhoGTPases such as Cdc42 and Rac have been shown to regulate or interact with both ephrins and integrins, and also to bind the filamin proteins (50–52). Moreover, the null *Flnc* mice show severe defects in myogenesis and myotube structure, which were similar in phenotype to the filamin-interacting, guanine exchange factor (GEF) TRIO (3,53) and these GEFs appear to modulate the RhoGTPases by binding filamin. Taken in sum, these observations would suggest an overriding model, whereby the signals from various surface receptors are mediated through the filamins, which in turn, regulate RhoGTPase activity through GEFs and lead to changes in actin polymerization. These various pathways involved in regulating the cytoskeleton provide a basis for the diverse phenotypes caused by loss of function of the filamin proteins.

MATERIAL AND METHODS

Only male mice were analyzed given the findings from the size and growth parameters observed on initial characterization. Despite the absence of clear growth and size differences, skeletal defects such as vertebral fusions and joint laxity were seen in the female null *Flnb* mice. All studies used greater than three mutant and three age-matched wild-type, littermate mice.

Generation of *Flnb* (−/−) mice

A 16 kb mouse genomic DNA fragment containing exons 3–5 of Flnb was cloned from the mouse 129Sv/Ev lamda genomic library. A 2.2 kb SpeI fragment, located 0.4 kb downstream of exon 5, was used to make the short arm of the targeting vector. The long arm is a 6 kb PCR fragment from primer 5′-TCTAAACAGGGCTGAGCACATGAC-3′ (6.1 kb upstream of exon 3) to primer 5′-CTAGGATCTGCTTCAGGGTC TCTG-3′ (120 bp upstream of exon 3). In this strategy, the Neo cassette replaced exon 3–5 of the filamin B gene. The

targeting vector was linearized by *Not*I and then transfected by electroporation of iTL1 (129/SvEv) embryonic stem cells. The recombinant clones were selected by G418 resistance and confirmed by Southern blot analysis. The correctly targeted ES cell lines were microinjected into the C57BL/6J blastocysts to produce chimeras. The chimeric mice were then set up for mating to generate germline *Flnb* (+/−) heterozygous mice. *Flnb* (−/−) homozygous mice were generated by heterozygous *Flnb* (−/+) matings. The genotype was confirmed by PCR of genomic toe DNA and protein phenotype by western blot analyses. The wild-type allele was detected by the primer pair 5′-AGATTATTCACCCGGACGTG-3′ and 5′-CCTGGGCTA ATAATGGCAGA-3′; and the mutated allele by 5′-CTGTG CTCGACGTTGTCACTG-3′ and 5′-GATCCCCTCAGAAGA ACTCGT-3′.

Body weight and growth curves

Five litters of mice from heterozygous matings were pooled and whole body weights were recorded in mice at 8 weeks of age. One wild-type, heterozygous and homozygous male mice each from the same litter was recorded every 2 days until 8 weeks old. The growth rate was calculated according to Wang *et al*. (19) as $p(1-p)$A/C, where $p =$ weight/A, A is the maximal weight for each individual mouse, C is a measure of relative growth rate, the difference of the numbers of days when the weight change from 1/2A to $1/(1+e-1)$A.

Micro-CT scan and measurement of Hounsfield units

Mice were sacrificed, perfused in 4% paraformaldehyde and scanned by micro-CT to evaluate bone structure and density changes using an eXploreLocus MicroCT (GE Healthcare London, Ontario). Hounsfield units were measured using the standard 2D Quantitative CT (QCT) methodology of measuring the densities of vertebral bodies T12 through L3. Regions of interest over the vertebral bodies were obtained using Efilm 2.1, using DICOM data generated from the CT scans. One millimeter axial images were utilized when available; when original axial images were unavailable, 1 mm axial images were generated through 3D multiplanar reconstruction. The CT scanner was initially calibrated to known bone and water standard densities. Thereafter, standards of known density were not imaged along with each set of mice. However, scans of homozygous, heterozygous and wild-type mice were performed simultaneously when size permitted. All images were obtained on the same scanner within a short period of time (hours) such that internal comparisons would be valid. An observer, blinded to the genotype of the mice, made the bone densitometry measurements.

Skeletal staining and histology

E18.5 embryos from wild-type and mutant mice were skinned and eviscerated, then dehydrated in 95% ethanol overnight, and acetone overnight; the embryos were then stained with Alizarin red (0.005%) and Alcian blue (0.015%) in a solution containing ethanol, glacial acetic acid and water (60:5:35) at 37°C overnight. The stained embryos were then transferred to1% potassium hydroxide solution for 2 days to dissolve the soft tissue; the cleared skeletons were preserved in glycerol (54). The upper limbs from wild-type and mutant mice were dissected after perfusing animals with 4% Paraformaldehyde (for normal histological staining) or 2% Paraformaldehyde/2% Glutaraldehyde (for electro microscope). After paraffin embedding and section, hematoxylin and eosin (HE), safranin-O and von Kossa staining as well as EM were performed.

Immuno-stain and TUNEL-stain

Tissue sections after antigen retrieval or fixed cells were placed in blocking solution with PBS containing 10% fetal calf serum, 5% horse serum and 5% goat serum, incubated overnight in the appropriate antibody (Collagen II, MP Biomedicals; BrdU, Oxford Biotechnology; Phospho-histone H3, Upstate; Phospho-Integrinβ1, Affinity Bioreagents, pSer785), and processed through standard avidin/biotin amplification (Vectastain, Burlingame, CA, USA) or fluorescent secondaries (CY3, Jackson Immunoresearch Laboratories, Westgrove, PA, USA, and FITC, Sigma). Specimens were examined using through-light or fluorescence microscopy after mounting in appropriate media. For BrdU labeling, the pregnant mice or newborn mice were injected intraperitoneally with BrdU (100 mg/kg Roche) 1 h before sacrifice. Apoptosis were detected in sections by TUNEL using *In Situ* Cell Death Detection Kit, TMR red (Roche). Sections with positive stained cells were counted in at least three sections for each animal and 3–5 animals for each assay. Cells staining positive for expressed markers were counted with respect to the total number of cells in five randomly chosen microscopic fields (0.072 mm^2; magnification: 400×) across the long axis of each object; an average of 200 cells were sampled on each well and the results shown represent values from three wells per treatment.

In situ hybridization

Section *in situ* hybridization with digoxigenin labeled probes was performed as described (55). The collagen I, II and X, Ihh and Pthrp receptor probes have been previously described and were kindly provided by Bjorn Olson and Clif Tabin laboratorys.

Western blot

Proteins were extracted from liver or primary cultured chondrocytes from wild-type and mutant mice by previously described methods (9). Briefly, cells were solubilized in lysis buffer, separated on a 7.5% SDS–PAGE gel and transferred onto PVDF membrane. The membrane was probed with the appropriate antibody (FlnA/B Ab courtesy of Drs Stossel and Hartwig; Integrin β1: Affinity Bioreagents, pSer785) and detected by enhanced chemiluminescence.

Analysis of chondrocyte progression through the hypertrophic zone

Both experimental and control pregnant E16.5–E17.5 mice received intraperitoneal injections of BrdU(Roche) at 100 mg/kg body weight. Animals were sacrificed 1–12 h

after BrdU injection, the forearms were dissected and cryosections were collected. The sections were then stained with BrdU primary antibody, biotinylated-anti-rat secondary antibody and streptavidin-HRP/Alexa Flur 488 tyramide (Molecular Probes). Rates of proliferation and progressive differentiation toward the hypertrophic zone were quantified in the radius bones. The rate of proliferation was assessed by counting the number of BrdU cells relative to the total number of cell nuclei seen under Hoechst nuclear staining within the resting, proliferative and prehypertrophic zones. The longitudinal areas of the resting and proliferative zones were divided into four equal areas to assess for differences in proliferative within the different zones for the mutant and control mice. In most instances, the lengths of the resting and proliferative zones were similar for the control and experimental mice. The rate of chondrocyte progression and differentiation through the hypertrophic zone was gauged by quantifying the number of BrdU positive chondroctyes within each of the four areas relative to the total number of BrdU positive cells at 12 h post-injection. At least five sections were counted for each animal and 3–5 animals were used for each assay.

GST protein interaction assay for β1-integrin and FlnB

GST-β1 integrin and empty GST vector were transfected into DH5α, expanded in 100 ml LB medium induced by IPTG (0.3 mM). The bacteria were collected by centrifugation and sonicated in 10 ml ice-cold 1× PBS, 1× proteinase inhibitor and 1% Triton X-100. Glutathione–Sepharose 4B beads were equilibrated in PBS and mixed with one volume of bacterially expressed GST fusion proteins on a rotary shaker for 60 min at RT. The beads were washed three times with 10 volumes of PBS and equilibrated in washing buffer [20 mM Hepes (pH 7.9), 100 mM KCl, 5 mM $MgCl_2$, 0.2% Nonidet P-40, 2 mM phenylmethylsulfonyl fluoride, 10 μg/ml aprotinine). Two hundred microliters of a bead slurry was combined with 1 ml of cultured 293 cells transfected with myc-FLNA (amino acid 2163–2647) or myc-FLNB (amino acid 2121–2602) pcDNA4 constructs. The beads were then washed five times with 20 volumes of washing buffer, and the bound proteins were eluted by boiling in Laemmli SDS–PAGE loading buffer and subjected to SDS–PAGE. Bound proteins were visualized by western blotting.

Chondrocyte cultures

Primary chondrocytes from growth plates of newborn mice were prepared according to the Lefebvre's protocol (56). Briefly, the growth plates of radius and ulna were dissected from P7 mice, minced and washed in cold Hanks buffered saline solution, and placed in 0.2% Collagenase Type I (Worthington, Lakewood, NJ) solution in DMEM at 37°C for 2 h. Soft tissues were detached from cartilage by repeated pipetting; the sediment cartilage was further digested with 0.2% Collagenase I for 6 h. The dissociated cells were then passed through a cell strainer to isolate single cells and were plated at feasible density in DMEM with 10% FBS. The cultures were maintained in a 37°C/5% CO_2 incubator for 2 days prior to analysis for adhesion and loss of integrin function through transfection experiments. Transfections of the dominant negative β1- integrin construct (courtesy Dr Robert Burke) were performed using lipofectamine (Invitrogen) according to the manufacturer's suggested protocols. The construct includes the full-length hemagglutinin extracellular and transmembrane domains, followed by GCCATGGCG and then the amino acids KLLM of the Xenopus β1- integrin cytoplasmic tail. This sequence is cloned into a pCMS-EGFP vector (57).

Cell adhesion assay. The cell adhesion assay followed manufacturer's protocols (Chemicon ECM cell adhesion kit). Wild-type and *Flnb* −/− chondrocytes were plated in 96-well plates (Chemicon) coated with different adhesion ligands (collagen I, collagen II, collagen IV, fibronectin, laminin, tenascin, vitronectin), incubated in a 37°C/5% CO_2 incubator for 2 h. The culture medium was discarded and the cells were gently washed with assay buffer, stained with cell staining solution and incubated for 5 min, followed by washing with deionized water three times. The absorbance was determined at 550 nm on a microplate reader. Three replicates were performed for each ligand.

For determination of cell areas following transfection, chondrocytes were stained with phalloidin to assess the actin cytoskeleton. Random areas were then captured by digital fluorescence microscopy, and the cellular area of chondrocytes was circled according to phalloidin-stained boundaries and measured using NIH Image J software. At least 50 cells are measured for each sample, and three replicates performed for each treatment.

Electron microscopy

Electron microscopy studies followed previously described methods (58). The upper limbs from wild-type and mutant mice were dissected after perfusing animals with EM fixative (4% sucrose, 2.5% glutaraldehyde and 2% paraformaldehyde in piperazine diethanesulfonic acid buffer). Samples were osmicated with 1% osmium tetroxide, washed with PBS and washed with distilled water. Pellets were then placed in 1% uranyl acetate at room temperature, washed in distilled water and serially dehydrated in ethanol. One milliliter of propylene oxide was placed in each sample and then replaced with a 1 ml mixture of polypropylene oxide and accelerated Epon-Araldite (1:1, vol/vol). The solution was replaced with 1 ml Epon-Araldite and placed in a 60°C oven overnight. Sections were cut at 50–100 nm, stained with uranyl acetate and lead citrate and examined with a transmission electron microscope (JEOL, Peabody, MA).

ACKNOWLEDGEMENTS

We thank Drs Clifford Tabin and Amitabha Bandyopadhyay for technical help, Prof. Bjorn Olson for the collagen probes, Prof. Robert Burke for supplying the dominant negative β1-integrin construct and Drs Thomas Stossel and John Hartwig for kindly providing filamin A/B antibodies. This work was supported by grants to C.W. (for Christopher Walsh) from the NINDS (2R37 NS35129 and 1PO1NS40043). C.W. is an Investigator of the Howard Hughes Medical Institute. V.S.

(for Volney Sheen) is supported by grants from Julian and Carol Cohen, the NIMH (1K08MH/NS63886–01), the Milton Fund and the Ellison Fund. V.S. is a Charles A. Dana fellow and a Beckman Young Investigator.

Conflict of Interest statement. None declared.

REFERENCES

1. Hartwig, J.H., Niederman, R. and Lind, S.E. (1985) Cortical actin structures and their relationship to mammalian cell movements. *Subcell. Biochem.*, **11**, 1–49.
2. Feng, Y. and Walsh, C.A. (2004) The many faces of filamin: a versatile molecular scaffold for cell motility and signalling. *Nat. Cell Biol.*, **6**, 1034–1038.
3. Dalkilic, I., Schienda, J., Thompson, T.G. and Kunkel, L.M. (2006) Loss of FilaminC (FLNc) results in severe defects in myogenesis and myotube structure. *Mol. Cell Biol.*, **26**, 6522–6534.
4. Hart, A.W., Morgan, J.E., Schneider, J., West, K., McKie, L., Bhattacharya, S., Jackson, I.J. and Cross, S.H. (2006) Cardiac malformations and midline skeletal defects in mice lacking filamin A. *Hum. Mol. Genet.*, **15**, 2457–2467.
5. Takafuta, T., Saeki, M., Fujimoto, T.T., Fujimura, K. and Shapiro, S.S. (2003) A new member of the LIM protein family binds to filamin B and localizes at stress fibers. *J. Biol. Chem.*, **278**, 12175–12181.
6. Takafuta, T., Wu, G., Murphy, G.F. and Shapiro, S.S. (1998) Human beta-filamin is a new protein that interacts with the cytoplasmic tail of glycoprotein Ibalpha. *J. Biol. Chem.*, **273**, 17531–17538.
7. van der Flier, A., Kuikman, I., Kramer, D., Geerts, D., Kreft, M., Takafuta, T., Shapiro, S.S. and Sonnenberg, A. (2002) Different splice variants of filamin-B affect myogenesis, subcellular distribution, and determine binding to integrin [beta] subunits. *J. Cell Biol.*, **156**, 361–376.
8. Zhang, W., Han, S.W., McKeel, D.W., Goate, A. and Wu, J.Y. (1998) Interaction of presenilins with the filamin family of actin-binding proteins. *J. Neurosci.*, **18**, 914–922.
9. Sheen, V.L., Feng, Y., Graham, D., Takafuta, T., Shapiro, S.S. and Walsh, C.A. (2002) Filamin A and Filamin B are co-expressed within neurons during periods of neuronal migration and can physically interact. *Hum. Mol. Genet.*, **11**, 2845–2854.
10. Stossel, T.P., Condeelis, J., Cooley, L., Hartwig, J.H., Noegel, A., Schleicher, M. and Shapiro, S.S. (2001) Filamins as integrators of cell mechanics and signalling. *Nat. Rev. Mol. Cell Biol.*, **2**, 138–145.
11. Krakow, D., Robertson, S.P., King, L.M., Morgan, T., Sebald, E.T., Bertolotto, C., Wachsmann-Hogiu, S., Acuna, D., Shapiro, S.S., Takafuta, T. *et al.* (2004) Mutations in the gene encoding filamin B disrupt vertebral segmentation, joint formation and skeletogenesis. *Nat. Genet.*, **36**, 405–410.
12. Jiang, Y., Zhao, J., Liao, E.Y., Dai, R.C., Wu, X.P. and Genant, H.K. (2005) Application of micro-CT assessment of 3-D bone microstructure in preclinical and clinical studies. *J. Bone Miner. Metab.*, **23** (suppl.), 122–131.
13. Provot, S. and Schipani, E. (2005) Molecular mechanisms of endochondral bone development. *Biochem. Biophys. Res. Commun.*, **328**, 658–665.
14. Bengtsson, T., Aszodi, A., Nicolae, C., Hunziker, E.B., Lundgren-Akerlund, E. and Fassler, R. (2005) Loss of alpha10beta1 integrin expression leads to moderate dysfunction of growth plate chondrocytes. *J. Cell Sci.*, **118**, 929–936.
15. Horiki, M., Imamura, T., Okamoto, M., Hayashi, M., Murai, J., Myoui, A., Ochi, T., Miyazono, K., Yoshikawa, H. and Tsumaki, N. (2004) Smad6/Smurf1 overexpression in cartilage delays chondrocyte hypertrophy and causes dwarfism with osteopenia. *J. Cell Biol.*, **165**, 433–445.
16. Long, F., Zhang, X.M., Karp, S., Yang, Y. and McMahon, A.P. (2001) Genetic manipulation of hedgehog signaling in the endochondral skeleton reveals a direct role in the regulation of chondrocyte proliferation. *Development*, **128**, 5099–5108.
17. St-Jacques, B., Hammerschmidt, M. and McMahon, A.P. (1999) Indian hedgehog signaling regulates proliferation and differentiation of chondrocytes and is essential for bone formation. *Genes Dev.*, **13**, 2072–2086.
18. Terpstra, L., Prud'homme, J., Arabian, A., Takeda, S., Karsenty, G., Dedhar, S. and St-Arnaud, R. (2003) Reduced chondrocyte proliferation and chondrodysplasia in mice lacking the integrin-linked kinase in chondrocytes. *J. Cell Biol.*, **162**, 139–148.
19. Wang, W.F., Wang, Y.G., Reginato, A.M., Plotkina, S., Gridley, T. and Olsen, B.R. (2002) Growth defect in Grg5 null mice is associated with reduced Ihh signaling in growth plates. *Dev. Dyn.*, **224**, 79–89.
20. Yoshida, C.A., Furuichi, T., Fujita, T., Fukuyama, R., Kanatani, N., Kobayashi, S., Satake, M., Takada, K. and Komori, T. (2002) Core-binding factor beta interacts with Runx2 and is required for skeletal development. *Nat. Genet.*, **32**, 633–638.
21. Yoshida, C.A., Yamamoto, H., Fujita, T., Furuichi, T., Ito, K., Inoue, K., Yamana, K., Zanma, A., Takada, K., Ito, Y. *et al.* (2004) Runx2 and Runx3 are essential for chondrocyte maturation, and Runx2 regulates limb growth through induction of Indian hedgehog. *Genes Dev.*, **18**, 952–963.
22. Komori, T., Yagi, H., Nomura, S., Yamaguchi, A., Sasaki, K., Deguchi, K., Shimizu, Y., Bronson, R.T., Gao, Y.H., Inada, M. *et al.* (1997) Targeted disruption of Cbfa1 results in a complete lack of bone formation owing to maturational arrest of osteoblasts. *Cell*, **89**, 755–764.
23. Mishina, Y., Starbuck, M.W., Gentile, M.A., Fukuda, T., Kasparcova, V., Seedor, J.G., Hanks, M.C., Amling, M., Pinero, G.J., Harada, S. *et al.* (2004) Bone morphogenetic protein type IA receptor signaling regulates postnatal osteoblast function and bone remodeling. *J. Biol. Chem.*, **279**, 27560–27566.
24. Zhao, M., Harris, S.E., Horn, D., Geng, Z., Nishimura, R., Mundy, G.R. and Chen, D. (2002) Bone morphogenetic protein receptor signaling is necessary for normal murine postnatal bone formation. *J. Cell Biol.*, **157**, 1049–1060.
25. Costell, M., Gustafsson, E., Aszodi, A., Morgelin, M., Bloch, W., Hunziker, E., Addicks, K., Timpl, R. and Fassler, R. (1999) Perlecan maintains the integrity of cartilage and some basement membranes. *J. Cell Biol.*, **147**, 1109–1122.
26. Watanabe, H. and Yamada, Y. (1999) Mice lacking link protein develop dwarfism and craniofacial abnormalities. *Nat. Genet.*, **21**, 225–229.
27. Ye, L., Mishina, Y., Chen, D., Huang, H., Dallas, S.L., Dallas, M.R., Sivakumar, P., Kunieda, T., Tsutsui, T.W., Boskey, A. *et al.* (2005) Dmp1-deficient mice display severe defects in cartilage formation responsible for a chondrodysplasia-like phenotype. *J. Biol. Chem.*, **280**, 6197–6203.
28. Aszodi, A., Hunziker, E.B., Brakebusch, C. and Fassler, R. (2003) Beta1 integrins regulate chondrocyte rotation, G1 progression, and cytokinesis. *Genes Dev.*, **17**, 2465–2479.
29. Loeser, R.F., Sadiev, S., Tan, L. and Goldring, M.B. (2000) Integrin expression by primary and immortalized human chondrocytes: evidence of a differential role for alpha1beta1 and alpha2beta1 integrins in mediating chondrocyte adhesion to types II and VI collagen. *Osteoarthritis Cartilage*, **8**, 96–105.
30. Giancotti, F.G. and Ruoslahti, E. (1999) Integrin signaling. *Science*, **285**, 1028–1032.
31. Hynes, R.O. (2002) Integrins: bidirectional, allosteric signaling machines. *Cell*, **110**, 673–687.
32. Mulrooney, J.P., Hong, T. and Grabel, L.B. (2001) Serine 785 phosphorylation of the beta1 cytoplasmic domain modulates beta1A-integrin-dependent functions. *J. Cell Sci.*, **114**, 2525–2533.
33. Bicknell, L.S., Morgan, T., Bonafe, L., Wessels, M.W., Bialer, M.G., Willems, P.J., Cohn, D.H., Krakow, D. and Robertson, S.P. (2005) Mutations in FLNB cause boomerang dysplasia. *J. Med. Genet.*, **42**, e43.
34. Biesecker, L.G. (2004) Phenotype matters. *Nat. Genet.*, **36**, 323–324.
35. Akbarnia, B.A. and Moe, J.H. (1978) Familial congenital scoliosis with unilateral unsegemented bar. Case report of two siblings. *J. Bone Joint Surg. Am.*, **60**, 259–261.
36. Ventruto, V. and Catani, L. (1986) New syndrome: progressive scoliosis by unilateral unsegmented fusion bar, foot deformity, joint laxity, congenital inguinal herniae, peculiar face. *Am. J. Med. Genet.*, **25**, 429–432.
37. Wiles, C.R., Taylor, T.F. and Sillence, D.O. (1992) Congenital synspondylism. *Am. J. Med. Genet.*, **42**, 288–295.
38. Kozlowski, K., Tsuruta, T., Kameda, Y., Kan, A. and Leslie, G. (1981) New forms of neonatal death dwarfism. Report of 3 cases. *Pediatr. Radiol.*, **10**, 155–160.
39. Farrington-Rock, C., Firestein, M.H., Bicknell, L.S., Superti-Furga, A., Bacino, C.A., Cormier-Daire, V., Le Merrer, M., Baumann, C., Roume, J.,

Rump, P. *et al.* (2006) Mutations in two regions of FLNB result in atelosteogenesis I and III. *Hum. Mutat.*, **27**, 705–710.
40. Harris, R. and Cullen, C.H. (1971) Autosomal dominant inheritance in Larsen's syndrome. *Clin. Genet.*, **2**, 87–90.
41. Larsen, L.J., Schottstaedt, E.R. and Bost, F.C. (1950) Multiple congenital dislocations associated with characteristic facial abnormality. *J. Pediatr.*, **37**, 574–581.
42. Zhou, X., Tian, F., Sandzen, J., Cao, R., Flaberg, E., Szekely, L., Cao, Y., Ohlsson, C., Bergo, M.O., Boren, J. *et al.* (2007) Filamin B deficiency in mice results in skeletal malformations and impaired microvascular development. *Proc. Natl Acad. Sci. USA*, **104**, 3919–3924.
43. Calderwood, D.A., Huttenlocher, A., Kiosses, W.B., Rose, D.M., Woodside, D.G., Schwartz, M.A. and Ginsberg, M.H. (2001) Increased filamin binding to beta-integrin cytoplasmic domains inhibits cell migration. *Nat. Cell Biol.*, **3**, 1060–1068.
44. Garciadiego-Cazares, D., Rosales, C., Katoh, M. and Chimal-Monroy, J. (2004) Coordination of chondrocyte differentiation and joint formation by alpha5beta1 integrin in the developing appendicular skeleton. *Development*, **131**, 4735–4742.
45. Hirsch, M.S., Lunsford, L.E., Trinkaus-Randall, V. and Svoboda, K.K. (1997) Chondrocyte survival and differentiation *in situ* are integrin mediated. *Dev. Dyn.*, **210**, 249–263.
46. Grashoff, C., Aszodi, A., Sakai, T., Hunziker, E.B. and Fassler, R. (2003) Integrin-linked kinase regulates chondrocyte shape and proliferation. *EMBO Rep.*, **4**, 432–438.
47. van der Flier, A. and Sonnenberg, A. (2001) Function and interactions of integrins. *Cell Tissue Res.*, **305**, 285–298.
48. Liu, G., Thomas, L., Warren, R.A., Enns, C.A., Cunningham, C.C., Hartwig, J.H. and Thomas, G. (1997) Cytoskeletal protein ABP-280 directs the intracellular trafficking of furin and modulates proprotein processing in the endocytic pathway. *J. Cell Biol.*, **139**, 1719–1733.
49. Wieland, I., Jakubiczka, S., Muschke, P., Cohen, M., Thiele, H., Gerlach, K.L., Adams, R.H. and Wieacker, P. (2004) Mutations of the ephrin-B1 gene cause craniofrontonasal syndrome. *Am. J. Hum. Genet.*, **74**, 1209–1215.
50. Fukata, M., Nakagawa, M., Kuroda, S. and Kaibuchi, K. (1999) Cell adhesion and Rho small GTPases. *J. Cell Sci.*, **112**, 4491–4500.
51. Noren, N.K. and Pasquale, E.B. (2004) Eph receptor-ephrin bidirectional signals that target Ras and Rho proteins. *Cell Signal.*, **16**, 655–666.
52. Ohta, Y., Suzuki, N., Nakamura, S., Hartwig, J.H. and Stossel, T.P. (1999) The small GTPase RalA targets filamin to induce filopodia. *Proc. Natl Acad. Sci. USA*, **96**, 2122–2128.
53. Bellanger, J.M., Astier, C., Sardet, C., Ohta, Y., Stossel, T.P. and Debant, A. (2000) The Rac1- and RhoG-specific GEF domain of Trio targets filamin to remodel cytoskeletal actin. *Nat. Cell Biol.*, **2**, 888–892.
54. McLeod, M.J. (1980) Differential staining of cartilage and bone in whole mouse fetuses by alcian blue and alizarin red S. *Teratology*, **22**, 299–301.
55. Brent, A.E., Schweitzer, R. and Tabin, C.J. (2003) A somitic compartment of tendon progenitors. *Cell*, **113**, 235–248.
56. Lefebvre, V., Garofalo, S., Zhou, G., Metsaranta, M., Vuorio, E. and De Crombrugghe, B. (1994) Characterization of primary cultures of chondrocytes from type II collagen/beta-galactosidase transgenic mice. *Matrix Biol.*, **14**, 329–335.
57. Marsden, M. and DeSimone, D.W. (2001) Regulation of cell polarity, radial intercalation and epiboly in *Xenopus*: novel roles for integrin and fibronectin. *Development*, **128**, 3635–3647.
58. Sheen, V.L. and Macklis, J.D. (1994) Apoptotic mechanisms in targeted neuronal cell death by chromophore-activated photolysis. *Exp. Neurol.*, **130**, 67–81.